High-resolution global shipping emission inventory by Shipping Emission Inventory Model (SEIM)

Wen Yi [1]†, Xiaotong Wang [2]†, Tingkun He [1], Huan Liu [1*], Zhenyu Luo [1], Zhaofeng Lv [1], Kebin He [1]

[1] State Key Joint Laboratory of ESPC, School of Environment, Tsinghua University, Beijing 100084, China

[2] Key Laboratory of Beijing on Regional Air Pollution Control, Beijing University of Technology, Beijing 100124, China

[*] Correspondence to: liu_env@tsinghua.edu.cn (H. Liu)

† These authors contributed equally to this work

Abstract: The high-resolution ship emission inventory serves as a crucial dataset for various disciplines including atmospheric science, marine science, environmental management, etc. Here, we present a global high spatiotemporal resolution ship emission inventory at a resolution of $0.1° \times 0.1°$ for the years 2013, 2016-2021, generated by the state-of-the-art Shipping Emission Inventory Model (SEIMv2.2). Initially, the annual 30 billion Automatic Identification System (AIS) data underwent extensive cleaning to ensure data validity and accuracy in temporal and spatial distribution. Subsequently, integrating real-time vessel positions and speeds from AIS data with static technical parameters, emission factors, and other computational parameters, SEIM simulated ship emissions on a ship-by-ship, signal-by-signal basis. Finally, the results were aggregated and analyzed. In 2021, the ship activity dataset established based on AIS data covered 109.3 thousand vessels globally (101.4 thousand vessels reported by the United Nations Conference on Trade and Development). Concerning the major air pollutants and greenhouse gases, global ships emitted 847.2 million tons of CO_2, 2.3 million tons of SO_2, 16.1 million tons of NO_x, 791.2 kilo tons of CO, 737.3 kilo tons of HC, 415.5 kilo tons of primary $PM_{2.5}$, 61.6 kilo tons of BC, 210.3 kilo tons of CH_4, 45.1 kilo tons of N_2O in 2021, accounting for 3.2% of SO_2, 14.2% of NO_x, and 2.3% of CO_2 emissions from all global anthropogenic sources, based on the Community Emissions Data System (CEDS). Due to the implementation of fuel-switching policies, global ship emissions of SO_2 and primary $PM_{2.5}$ saw a significant reduction of 81.3% and 76.5% in 2021 compared to 2019, respectively. According to the inventory results, the composition of vessel types contributing to global ship emissions remained

relatively stable through the years, with container ships consistently contributing ~ 30% of global ship

30 emissions. Regarding vessel age distribution, the emission contribution of vessels built before 2000

(without Tier standard) has been declining, dropping to 10.2% in 2021, suggesting that even a complete

phase-out of these vessels would have limited potential for reducing NOx emissions in the short term.

On the other hand, the emission contribution of vessels built after 2016 (meeting Tier III standard) kept

increasing, reaching 13.3% in 2021. Temporally, global ship emissions exhibited minimal daily

35 fluctuations. Spatially, high-resolution emission characteristics of different vessel types were delineated.

Patterns of ship emission contributions by different types of vessels vary among maritime regions, with

container ships predominant in the North and South Pacific, bulk carriers predominant in the South

Atlantic, and oil tankers prevalent in the Arabian Sea. The distribution characteristics of ship emissions

and intensity also vary significantly across different maritime regions. Our dataset, which is accessible

40 at https://zenodo.org/records/11069531 (Wen et al., 2024), provides daily breakdown by vessel type and

age is available for broad research purposes, and it will provide a solid data foundation for fine-scale

scientific research and shipping emission mitigation.

1   Introduction

Ships carry over 80% of global trade volume(Development, 2023). Employing heavy fuel oil, ships

45 emit significantly more atmospheric pollutants than diesel cars each year(Corbett et al., 1999; Endresen

et al., 2003; Jasper Faber, 2020). Existing studies indicate that ship emissions of atmospheric pollutants

and greenhouse gases have important environmental and climatic impacts on multiple spheres of the

Earth (Browse et al., 2013; Chen et al., 2020; Diamond, 2023; Zhang et al., 2021). In terms of air quality,

ships are regarded as a major source of $PM_{2.5}$ pollution in coastal cities (Liu et al., 2024; Luo et al., 2023).

50 Recent studies show that although ship emissions have decreased due to stricter control measures in

recent years, shipping-related mortality associated with long-term $PM_{2.5}$ exposure in Chinese coastal

areas increased by 11.4% from 2016 to 2020 as populations migrate towards coastal cities (Luo et al.,

2024). Ship emission-induced sulfur oxides aerosols, significantly influence local climates (Liu et al.,

2016; Yuan et al., 2022). With the increasing navigation in the Arctic, ship emissions of black carbon

55 have become a focal point of research and policy debates regarding their impact on the polar ice surface (Stephenson et al., 2018; Zhang et al., 2019). Regarding their impact on marine organisms, anthropogenic emissions account for over 80% of the utilizable nitrogen deposition in the ocean, with maritime emissions contributing to 15% of global NO_x emissions (Zhang et al., 2021). Given these facts, characterizing ship emissions is crucial for fundamental research in atmospheric, marine, and climatic

60 sciences, etc.

The characterization of ship emissions through emission inventories stands as a pivotal and effective methodology within maritime emissions research (Liu et al., 2016; Liu et al., 2024; Wang et al., 2021). Over the past 30 years, with the improvement of ship activity data collection mechanisms, the establishment of ship emission inventories has gradually shifted from the "top-down" approach, based

65 on fuel or power consumption statistics and empirical parameters, to the "bottom-up" approach, based on high spatiotemporal resolution shipping trajectory data (Eyring et al., 2010; Jasper Faber, 2020; Liu et al., 2016). Currently, the establishment of high spatiotemporal resolution ship emission inventories based on Automatic Identification System (AIS) data has become the most popular tool for scientific research and policy management in the field of ship emissions (Johansson et al., 2017; Kramel et al.,

70 2021; Wang et al., 2021). Leveraging real-time ship speed derived from AIS data along with vessel technical specifications such as deadweight tonnage and design speed, and emission factors, it is feasible to model instantaneous ship emissions and then aggregate them at a defined spatiotemporal granularity, thereby constructing a high-resolution emission inventory dataset. The advantage of this method is that the derived emission inventory does not rely on external spatiotemporal allocation parameters, but retains

75 accurate spatiotemporal information of ship emissions from AIS data (Liu et al., 2016). However, the challenge lies in the difficulty of processing AIS data, the complexity of simulating instantaneous ship emissions, and the significant computational resources required (Chen and Yang, 2024). Currently, the mainstream international ship emission inventory models based on AIS data include the Ship Traffic Emission Assessment Model (STEAM)(Jalkanen et al., 2012; Johansson et al., 2017) , the Shipping

80 Emission Inventory Model (SEIM), International Maritime Organization (IMO) emission inventory

model (Jasper Faber, 2020), Maritime Transport Environmental Assessment Model (MariTEAM) (Kramel et al., 2021), etc.

In this study, we established a 0.1° × 0.1° global daily ship emission inventory for the years 2013, 2016-2021 based on SEIMv2.2. This dataset covers five air pollutants (NO_x, SO_2, $PM_{2.5}$, CO, HC) and

85 four greenhouse gases (CO_2, CH_4, N_2O, BC). Due to rigorous quality control, the ship emission inventory established by SEIM possesses high information density, allowing for analysis across multiple dimensions, such as fleet structure and spatiotemporal characteristics. Initially, we conducted meticulous data cleaning and rigorous quality control on the commercially obtained global ship AIS data to establish a reliable ship activity dataset. Subsequently, employing the latest emission factor and real-time engine

90 power simulation methods for ships, SEIMv2.2 computed instantaneous ship emissions, integrating multiple quality control techniques such as interpolation processing for sparse routes and safety margin considerations to ensure the accuracy of ship emission simulation. Finally, we aggregated ship emissions from different temporal and spatial scales, as well as from different types and ages of ships. The derived high-resolution global shipping emission inventory could serve as input data for climate or atmospheric

95 chemistry models.

The next section will elucidate the methodology and factors employed in establishing our high-resolution ship emission inventory. Section 3.1 compares our results with previous global ship emission inventories. Section 3.2 analyzes the temporal sequence of global ship emissions. Section 3.3 examines the spatial distribution characteristics of global ship emissions. Section 4 provides information regarding

100 our dataset and data availability. Finally, Section 5 presents the conclusion.

2 Methods

2.1 Ship Emission Inventory Model (SEIM)

2.1.1 General principles

The Shipping Emission Inventory Model (SEIM) was first established by (Liu et al., 2016) based on the

105 idea of disaggregated dynamic method. Driven by AIS data, combined with each vessel's registration information, SEIM realized real-time, vessel-by-vessel shipping emission simulations. SEIM is suitable

for the establishment of multi-scale shipping emission inventories with applications on regions (Liu et al., 2016; Wang et al., 2021) and ports (Fu et al., 2017). SEIM has undergone two major updates: SEIMv2.0 (Wang et al., 2021) and SEIMv2.2 (this study). Compared to SEIMv2.0, SEIMv2.2 features

110 three key improvements. (1) IMO numbers are employed as the primary identifier to match AIS data and Ship Technical Specifications Database (STSD), and for those that cannot be matched, MMSI codes are used as the sencondary identifier. We found that the matching rate of the ship archive database established in previous years could significantly decrease when applied to new years. This is because when ships are leased or AIS equipment is replaced, the MMSI code often changes, while the IMO code

115 remains constant. Therefore, using the IMO code as the first-choice identifier ensures more accurate matching of AIS data and static ship information. See Sect. 2.1.2 for details. (2) The formula for calculating the main engine load has been revised to include parameterized correction schemes for draft, meteorological conditions, and hull fouling. Additionally, a main engine load maximum limit of 98% is set to consider the navigation safety of ships. Refer to Sect. 2.1.3 for further details. (3) The ship emission

120 factors are comprehensively updated according to the Fourth Green House Gases Study by IMO (Jasper Faber, 2020), and a black carbon calculation module has been integrated. This update also integrates the Emission Control Area (ECA) module correction module directly into the calculation process, rather than applying it as a post-process adjustment. Detailed methods are provided in Sect. 2.1.4. During the development of SEIMv2.2, SEIMv2.1 was derived, which only updated the emission factors compared

125 to SEIMv2.0. Generally, the technical scheme of SEIMv2.2 is illustrated in Fig. 1.
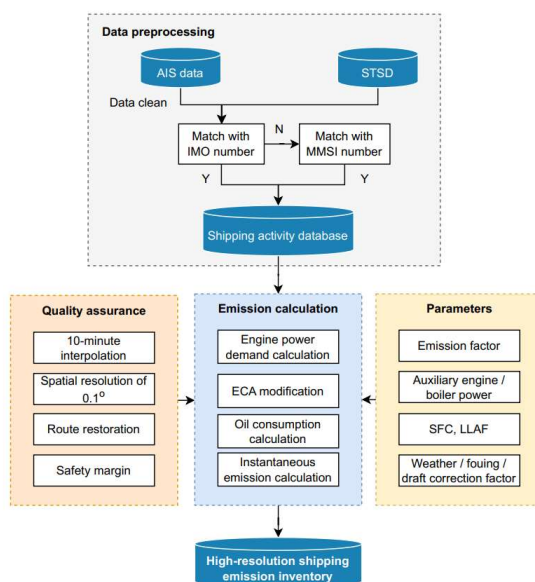
Figure 1: The technical scheme for SEIMv2.2

The calculation process and principles of SEIMv2.2 could be described as follows: Firstly, the original AIS data collected are subjected to cleaning, missing data filling, etc., to establish a well-cleaned dynamic AIS database. Secondly, IMO or MMSI codes are used as unique identifiers to match AIS data with the STSD, which provides essential technical parameters such as vessel type, deadweight tonnage, main engine power rating, design speed, etc., to establish a comprehensive shipping activity database. For the details of STSD, refer to (Wang et al., 2021). This study has incorporated information on newly built vessels from 2019 to 2021, obtained from the Lloyd's Register, into the established STSD. Thirdly, a series of parameters such as emission factors, auxiliary engine and boiler output power, specific fuel consumption, low load adjustment factors, and weather and fouling factors are input for ship emission simulation. Then, the model will calculate GHG and air pollutant emissions for every ship by every two subsequent AIS signals. The emissions from the main engine, auxiliary engine, and boiler are simulated using the corresponding formulas presented as Equation (1) - (3).

$$E_{ME,i,n,p} = P_{ME,i,n} \times EF_{ME,i,p} \times LLAF_{i,n,p} \times \Delta T_{i,n} \times 10^{-6} \qquad (1)$$

140

$$E_{AE,i,n,p} = P_{AE,i,n} \times EF_{AE,i,p} \times \Delta T_{i,n} \times 10^{-6} \qquad (2)$$

$$E_{B,i,n,p} = P_{B,i,n} \times EF_{B,i,p} \times \Delta T_{i,n} \times 10^{-6} \qquad (3)$$

Where the subscripts ME, AE, and B represent the main engine, auxiliary engine, and boiler, respectively; i represents individual ship; n represents the n-th AIS signals in the sequence, and the total number of AIS signals transmitted by the ship i could be expressed using Ni; p represents species of GHGs or air

145 pollutants. As for the capital letters, E represents the emissions of GHGs or air pollutants (unit: ton); EF is the emission factors (unit: g/kwh); P is the output power (unit: kw); ΔT is the time interval of two subsequent AIS signals (unit: h); LLAF is the low load adjust factor, which is applied only when the main engine load factor is lower than 20%, consistent with our previous work. The total emissions are calculated by summing up the emissions from all main engines, auxiliary engines, and boilers, as shown

150 in Equation (4).

$$E_{i,p} = \sum_{n=1}^{N_i-1} E_{i,n,p} = \sum_{n=1}^{N_i-1} (E_{ME,i,n,p} + E_{AE,i,n,p} + E_{B,i,n,p}) \qquad (4)$$

During the real-time calculation, linear interpolation is applied to latitude and longitude displacement as well as time intervals where the AIS time interval is greater than ten minutes. AIS latitude and longitude are rounded to one decimal place to ensure a spatial resolution of $0.1° \times 0.1°$. In the Chinese coastal region, route restoration technology is applied to restore routes crossing land, referred to (Wang et al.,

155 2021). If, due to anomalies in speed or other factors, the main engine load exceeds 100%, it is capped at 98% for safety navigation considerations. Finally, the high-resolution emission inventory generated by SEIM could be aggregated and analyzed from various angles such as emission structure, temporal variations, spatial distribution, etc., depending on study demands.

2.1.2 AIS data cleaning

160   AIS data provide high-density vessel activity data, including time, speed, and latitude-longitude coordinates. This study collected global shore-based and satellite-based AIS data, with an average annual signal count of approximately 30 billion. Due to irregular or erroneous information entry at ports or on vessels, as well as interference from complex marine environments, weather conditions, and terrain, AIS data may suffer from errors, duplicates, and losses. To enhance the accuracy of emission inventory

165   calculations, this study conducted meticulous cleaning of AIS data. Firstly, to ensure data validity, we filter AIS message records that met all of the following conditions: 1) Annual AIS signal count greater than 10; 2) Speed over ground less than 50 knots; 3) Longitudes ranged from -180° to 180° and latitudes ranged from -90° to 90°; 4) The timestamp of AIS signals within the target year.

Secondly, for temporal anomaly cleaning, signals with excessively long time intervals are filtered

170   out. According to the International Convention for the Safety of Life at Sea (SOLAS), vessels are required to maintain continuous transmission of AIS signals throughout the year, except for specific reasons permitted by regulations. Therefore, vessels theoretically maintain a high frequency of signal transmission during navigation. Taking the year 2021 as an example, Fig. S 3 reveals a distinct bimodal distribution of original AIS signals, with peaks occurring around 300 seconds and 2 hours. The peak of

175   around 300 seconds corresponds to the high-frequency interval for shore-based AIS equipment to receive signals, while the peak of around 2 hours mainly originates from satellite AIS signals. Statistical analysis shows that 99.6% of signal time intervals are within 8000 seconds. However, the total duration of these AIS signal intervals accounts for only 16% of all AIS signals, indicating the presence of extremely long consecutive signal intervals in the AIS data. This may be due to vessel docking for repairs or AIS

180   equipment malfunctions. To minimize uncertainty in emission calculations caused by these signals, this study filters out signals with time intervals exceeding 7 days, which are not included in the emission calculations.

Thirdly, for spatial distribution anomalies cleaning, AIS data distributed on land are filtered out. Spatial distribution of the annual original AIS signal (Fig. S 4) revealed a significant number of signals

185   deviating from shipping routes near the 0° and 120° meridians, located over Asia, Europe, and Africa.

Further analysis indicated that such abnormal signal points are caused by misaligned field information or data loss. To minimize the interference of these abnormal signals on emission calculations, this study employs the following cleaning methods: 1) For ships matched by IMO codes, signals with speeds >50 knots or consecutive latitude-longitude spans >20° are removed; 2) For ships matched by MMSI codes,

190   signals with speeds >40 knots or latitude-longitude spans >8° are excluded; 3) Signals located on land areas are excluded. Fig. S 4 simultaneously presents the spatial distribution of the cleaned AIS signals, revealing that signals on land near the 0° and 120° meridians have been eliminated while retaining signals on major navigable rivers in North America, South America, and Eurasia.

Fourthly, to ensure the reliability of ship technical parameter data matching, the AIS data are

195   subsequently aggregated and identified with IMO numbers and MMSI numbers. AIS data comprises static AIS data and dynamic AIS data. Static AIS data include time, MMSI numbers, IMO numbers, etc., but do not contain latitude and longitude information. Dynamic AIS data contain MMSI numbers and latitude and longitude information. This study integrates the static AIS data and dynamic AIS data by matching their common MMSI numbers. It is found that approximately 84% of the MMSI numbers in

200   dynamic information could be matched with a unique valid seven-digit IMO number. However, some ships may change their MMSI codes multiple times within a year. Data with MMSI code changes more than 10 times are excluded from emission calculations.

2.1.3   Engine power demand

Engine power demand is crucial for emission calculations. For the main engine, its real-time output

205   power is related to the main engine load, which can be depicted in real-time by changes in the ship's speed-over-ground obtained from AIS data. According to the propeller law, the main engine load factor is the cube of the ratio of the ship's actual speed to its design speed (Liu et al., 2016). Additionally, some studies indicate that factors such as draft, hydrological and weather conditions, and hull fouling also influence the main engine load (Chen and Yang, 2024; Emmens et al., 2021; Fu et al., 2022). Regarding

210   draft factors, the (Jasper Faber, 2020) corrects the main engine load using real-time draft data from AIS. However, draft fields in commercial AIS data are often manually recorded by crew members, leading to low accuracy and a large number of zero values. As for hydrological and weather conditions, wind and

waves could increase engine power demand through friction and shear resistance. (Johansson et al., 2017) adopts a method based on a real-time ship heading and weather field, which requires substantial computational resources and introduces greater uncertainty by the weather field. Additionally, the accumulation of micro- and macro-organisms on ship surfaces increases power demand to overcome resistance, and existing studies often use fixed parameters to correct the influence. This study introduces parameterization schemes to correct the influence of draft, weather, and hull fouling. Based on the ships' payload utilization calculation algorithm in (Imo, 2015), this study estimates the average drafts for different types of vessels, with specific values provided in Table S1. The correction coefficients for weather influences (η_w) are based on (Jasper Faber, 2020), also presented in Table S1. The correction coefficient for fouling influences (η_f) is set to 0.917. Specifically, the formula for calculating the real-time power of the main engine in SEIMv2.2 can be found in equation (5).

$$P_{ME,i,n} = P_{ref,i} \times LF_{i,n} = \frac{P_{ref,i} \times \left(\frac{D_i}{D_{ref,i}}\right)^{0.66} \times \left(\frac{v_{i,n}}{v_{ref,i}}\right)^3}{\eta_w \times \eta_f} \tag{5}$$

Where $P_{ref,i}$ represents the maximum engine output power (unit: kw) of the main engine of the ship i; $LF_{i,n}$ represents the main engine load factor of the ship i at the n-th AIS signals in the sequence. D_i represents the average draft; $D_{ref,i}$ represents the designed draft; $v_{i,n}$ represents the speed-over-ground (unit: knot) of the ship i at the n-th AIS signals in the sequence; $v_{ref,i}$ represents the design speed (unit: knot) of ship i, obtained from the static technical profiles; $\eta_{w,i}$ represents the weather correction factor and $\eta_{f,i}$ represents the fouling correction factor, both of which are unitless.

For auxiliary engines and boilers' power demand, this study adopts the recommended values from the IMO Fourth and Third Greenhouse Gas Study reports. Due to the lack of information, this study did not consider the impact of other auxiliary devices on board, such as solar panels, wind sails, waste heat recovery systems, and carbon capture, utilization and storage (CCUS) systems, on vessel energy consumption. These systems are not significant contributors to overall vessel energy consumption currently (Dnv, 2022). However, with the ongoing trends of energy efficiency improvements, the impact of these systems on vessel energy utilization could be transformative in the future (Kersey et al., 2022).

2.1.4 Emission factors

The emission factors applied by SEIMv2.0 is mainly based on the Third IMO GHG Study (Smith, 2014) as well as the National Standard for General Diesel Fuel of the People's Republic of China (Wang et al., 2021). In this study, we updated the emission factors based on the Forth IMO GHG Study (Jasper Faber, 2020), and therefore accompanying technical modification. Firstly, emission factors of conventional air pollutants (SO_2, NO_x, $PM_{2.5}$, CO, HC) and GHGs (CO_2, CH_4, N_2O) were updated. CO_2, SO_2, and $PM_{2.5}$ are considered typical species whose emission factors are highly dependent on the chemical component of fuels. Table. S2 represents the emissions factors based on fuel consumption for CO_2, SO_2, and $PM_{2.5}$. Energy-based emission factors are calculated based on fuel-based emission factors as well as specific fuel consumptions (SFC, unit: kwh/kg fuel), using Equation (6):

$$EF_e = EF_f \cdot SFC \qquad (6)$$

SFC represents the fuel consumption per unit of work performed by a ship, mainly decided by the fuel calorific value (kwh/kg fuel) and engine efficiency (%). During the operation of ships, energy efficiency could be considered as a quadratic function of the load factor of the main engine, generally with the optimal load factor of 80%. Equation (7) is applied to calculate the SFC for main engines based on the SFC under the optimal operating condition (SFC_{base}) and main engine load of the ship i.

$$SFC_{ME,i} = SFC_{base,ME,i} \cdot (0.455 \cdot LF_i^2 - 0.71 \cdot LF_i + 1.28) \qquad (7)$$

Generally, newer ships have a lower SFC_{base} than older ships due to the improvement of engine and auxiliary engine efficiency (Sou et al., 2022). The LNG fleet also has a lower SFC_{base} value than conventional fuel. SFC of auxiliary engines and boilers ($SFC_{AE|B,i}$) is not subject to the main engine load, so $SFC_{AE|B,base,i}$ is directly applied with no main engine load adjustment. Values of SFC_{base} are exhibited in Table. S 3.

Combining Table. S 2 and Equations (1), and (2), energy-based emission factors for the main engines of CO_2 and SO_2 as a function of the main engine load could be derived, as exhibited in Fig. S 1.

It could be noted that although Marine Gas Oil (MGO) has a higher carbon content compared to Heavy

260   Fuel Oil (HFO), its lower SFC results in a lower energy-based CO_2 emission factor. Fig. S 2 illustrates a

comparison between two algorithms employed in SEIMv2.0, which utilizes uniform emission factors for

all operational conditions, and SEIMv2.2, which incorporates load-dependent emission factors. We

selected a typical oil tanker with dead-water tonnage of 7562 tons and examined its hourly carbon

emissions from July 1 to July 15, 2019. It is evident that, at anchorage or berth, the hourly emissions

265   estimated by SEIMv2.2 are generally higher than or equal to those of the previous SEIMv2.0. When the

vessel is cruising, however, the overall emissions calculated by SEIMv2.2 are relatively lower compared

to SEIMv2.0. Emission factors of other air pollutants and GHGs in this study are shown in Table S 4 and

Table S 5.

2.2   Data source and quality control

270   ### 2.2.1   AIS data coverage

The AIS-observed data obtained in this study amounted to approximately 30 billion/year, while the

processed AIS signals after cleaning and interpolation averaged about 4-5 billion per year, with an

average annual operating time of approximately 5-7 million hours, as shown in Table 1. In comparison

to (Johansson et al., 2017), the AIS signal volume in this research is slightly lower, possibly due to

275   comprehensive quality control measures in data reduction and filtering, which removed a significant

number of signals with inadequate validity, abnormal time or spatial distribution, and insufficient

reliability. It can be observed that with the increasing prevalence of AIS equipment, the quantity of AIS

signals is on the rise. However, the operating time does not necessarily increase in proportion to the

signal quantity. The operating time decreased by 3.8% in 2020 compared to 2019 and increased by 4.5%

280   in 2021 compared to 2020, probably influenced by the pandemic,

Table 1: Annual AIS signals and operating time after data cleaning

Year	2013	2016	2017	2018	2019	2020	2021
AIS signals, billion	1.6	4.1	4.6	5.0	5.0	5.0	5.5
Operating time, million hour	225.8	578.5	643.6	700.9	693.8	667.3	697.6

Taking 2021 as an example, the spatial distribution of AIS signals after cleaning and time interpolation

285   is illustrated in Fig. 2. The spatial coverage of cleaned AIS signals is extensive, with signals primarily

concentrated along major shipping routes such as the coastal regions of East Asia, the Malacca Strait-

Cape of Good Hope route, the Mediterranean, and the Black Sea routes, effectively depicting the

trajectories of major shipping lanes.
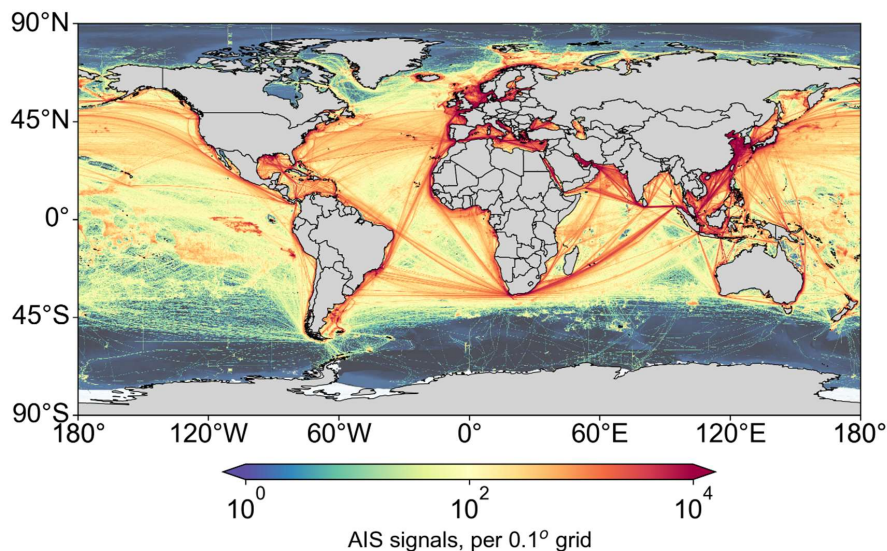
290   **Figure 2: The spatial distribution of global AIS signals in 2021. Maps are made with Natural Earth.**

2.2.2   Global fleet composition

Table 2 presents the global fleet structure obtained through matching AIS data with STSD in 2021. This study covers 14 vessel types, including major cargo vessels, passenger ships, and fishing vessels, along

295   with a category labeled "others," comprising research vessels, rescue ships, and work vessels, among others. Since the "others" category primarily consists of small coastal vessels, its contribution to emissions is minor. It's important to note that United Nations Conference on Trade and Development (UNCTAD) definition of "others" differs from this study's categorization. According to UNCTAD 2021 classification, other ships include liquefied petroleum gas carriers, liquefied natural gas carriers, parcel

300   (chemical) tankers, specialized tankers, reefers, offshore supply vessels, tugboats, dredgers, cruise ships, ferries, and other non-cargo ships. Moreover, it should be noted that the fleet obtained in this study comprises vessels with certain activity levels (annual AIS signals exceeding 10), whereas UNCTAD statistics do not consider vessel activity. This discrepancy might lead to comparatively lower results in this study.

305   Overall, the discrepancies between the global fleet statistics in this study and those of UNCTAD are not substantial. In terms of vessel numbers, this study reached 109.3 thousand in 2021, slightly higher than UNCTAD's 101.4 thousand. The total deadweight tonnage amounts to 1989.9 million tons, slightly lower than UNCTAD's 2136.2 million tons. Among the fleet obtained in this study, vessels matched by IMO numbers reach 62.9 thousand, contributing 57.5% of vessel count and 95.4% of deadweight tonnage.

310   Vessels matched by MMSI numbers constitute a larger proportion in count (42.5%), yet make a smaller contribution in deadweight tonnage (4.6%), predominantly consisting of fishing vessels (which contribute 87.9% to the vessel count matched by MMSI numbers). There's a noticeable difference in the quantity of general cargo ships and oil tankers. However, in terms of total tonnage, the container ships, general cargo ships, bulk carriers, and oil tankers show no significant differences (below 10%) with

315   UNCTAD, ensuring the reliability of global ship emission calculations and emission structure analysis.

Table 2: Comparison of the global fleet structure of this study and the UNCTAD statistics in 2021. The fleet analyzed in this study was filtered to include vessels with an annual AIS signal count greater than 10.

Vessel type	Number of vessels, thousand				Total deadweight tonnage, million ton			
	This study			UNCTAD	This study			UNCTAD
	match with IMO number	match with MMSI number	total		match with IMO number	match with MMSI number	total	
Auto Carrier	0.8	0.1	0.8		15.3	0.9	16.2	
Bulk Carrier	11.1	0.6	11.7	12.3	842.3	27.6	869.9	913.2
Chemical Tanker	4.7	0.3	5.0		100.5	4.5	105.0	
Container	4.2	0.3	4.5	5.4	218.8	14.4	233.2	281.8
Cruise	0.2	0.1	0.2		0.1	0.0	0.1	
Fishing ship	5.1	40.8	45.8		4.0	5.8	9.7	
General Cargo	6.9	0.8	7.7	20.0	66.4	4.4	70.7	77.9
LNG	0.3	0.0	0.3		19.3	0.2	19.5	
LPG	1.2	0.1	1.2		19.0	0.8	19.9	
Miscellaneous	12.3	1.4	13.7		76.1	6.5	82.6	
Ocean Tug	7.0	0.9	7.9		13.4	1.6	15.0	
Oil Tanker	5.4	0.4	5.8	11.5	505.3	22.2	527.5	619.3
Reefer	0.5	0.0	0.5		3.5	0.2	3.7	
Ro Ro	3.0	0.6	3.6		11.8	1.7	13.5	
Others	0.5	0.0	0.5	52.2	3.1	0.0	3.1	243.9
Total	62.9	46.4	109.3	101.4	1899.1	90.8	1989.9	2136.2

320 **3   Results**

3.1   Total global shipping emissions
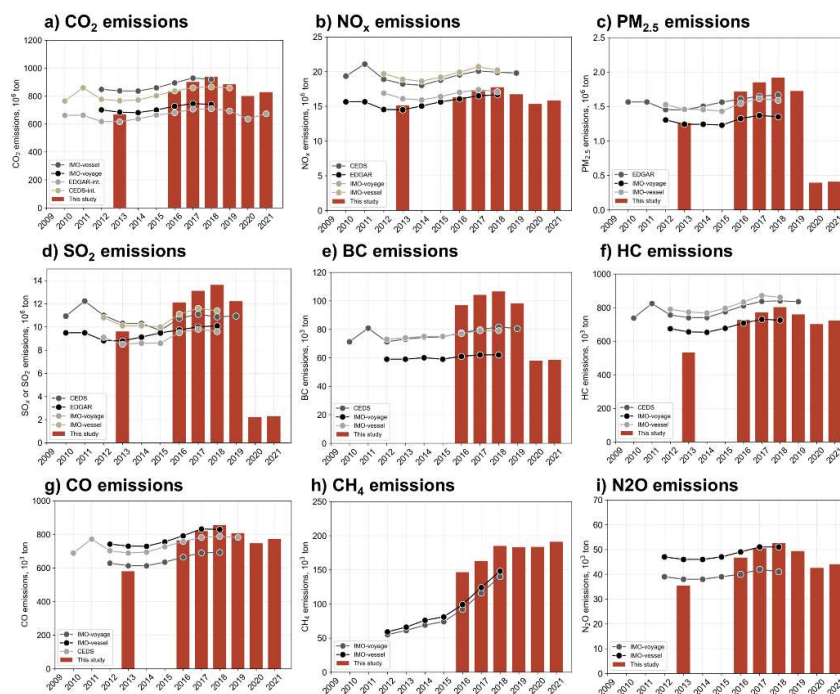
Figure 3: Global trends in shipping emissions from 2010 to 2021. Data source: IMO (Jasper Faber, 2020),
where IMO-Voyage results were calculated based on a voyage-based method and IMO-Vessel on a vessel-based
325   algorithm. Community Emissions Data System (Mcduffie et al., 2020); Emissions Database for Global
Atmospheric Research (Crippa, 2021).

We established a multi-year global ship emissions inventory with temporal resolution of day and
spatial resolution of 0.1^o using the SEIM model for the years 2013 and 2016-2021. Figure 3 summarizes
this study and open-source dataset of major atmospheric pollutants and greenhouse substances emitted
330   by global shipping over the past decade. The ship emission calculation method employed in this research,
which is AIS-based, aligns with those utilized in the EDGAR inventory and the Fourth IMO GHG Study
released in 2020, while the CEDS inventory is established based on a top-down fuel-based approach
(Mcduffie et al., 2020). Methodologically, our study is more comparable to the research conducted by
EDGAR and IMO, with the results from the CEDS inventory as a reference. It is important to note that

335   the SEIM model has undergone two major version updates. The data of different versions are presented in Figure S3. Figure 3 presents the integrated results for ease of comparison with other studies. Specifically, the results for 2013 are based on SEIMv1.0, while those for 2016-2020 are based on SEIMv2.1 and those for 2021 are based on SEIMv2.2.Due to slight differences between the two versions (Fig. S5), both of which include data for 2020, the total emissions for 2020 in SEIMv2.2 were adjusted

340   to match those in SEIMv2.1. The growth rate for 2021 was kept consistent to ensure that the data for both versions align in 2020. . In terms of annual emission totals, this study's results show similarities in emission trends and total emissions compared to well-known inventories such as EDGAR and IMO. For most species, this study's results show higher annual growth rates compared to IMO and EDGAR studies. For instance, this study estimates a 6.1% annual increase rate in global ship CO_2 emissions from 2016 to

345   2018, while IMO's study indicates only a 1.4% annual increase for its "vessel-based" results and 0.9% for its "voyage-based" results. In 2019 and 2020, influenced by international trade conflicts and the global pandemic, this study estimates a 5.8% and 9.5% year-on-year decrease in global ship CO_2 emissions for 2019 and 2020, respectively. In contrast, the year-on-year decrease rate estimated by EDGAR inventory is 2.1% and 8.4% for 2019 and 2020, respectively. Differences between studies may

350   stem from factors such as AIS data quality, coverage of static information, and factors considered in emission calculations. In 2020, the global implementation of the fuel-switching policy led to a significant reduction in the sulfur content of ship fuel. According to SEIM, in 2020 relative to 2019, SO_2, $PM_{2.5}$, and BC emissions decreased by 81.9%, 77.2%, and 40.9%, respectively. In 2021, following the recovery in global trade demand after the pandemic, this study estimates an increase of 3.5% in global ship CO_2

355   emissions compared with 2020, while EDGAR inventory estimates an increase of 5.9%. However, the latest data on ship's atmospheric pollutants from other inventories only extend to 2019, which is insufficient for comparing emission results with this study.

3.2 Temporal evolutions

3.2.1 Daily shipping emissions
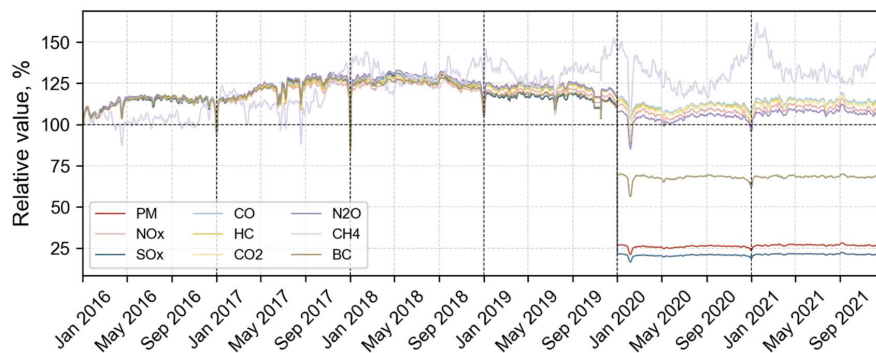
360

Figure 4: Daily global shipping air pollutants and GHG emissions from 2016 to 2021. With January 1, 2016, as the reference point, the five-day moving average of daily relative emissions is displayed.

To compare the magnitude of changes in emissions of various atmospheric pollutants and greenhouse gases emitted by ships, Fig. 4 converts the daily ship emissions of 9 species into daily relative

365 quantities taking the emission levels on January 1, 2016, as the reference point. Figure 4 reveals that, aside from occasional sharp declines or increases on certain dates, the daily variations in ship emissions are generally stable. This suggests that the emission simulations by the SEIM model exhibit continuity and stability. Ships typically cruise at constant speeds on high seas without significant diurnal or other periodic variations, so global ship emissions do not exhibit pronounced daily or seasonal fluctuations.

370 Any anomalies such as sudden drops or spikes may be attributed to signal transmission anomalies in equipment or meteorological factors. In 2019, the reduction in ship SO_2 emissions compared to 2018 was slightly larger than that of other pollutants, probably attributed to the implementation of the domestic emission control area policy within 12 nautical miles of the Chinese coast, one of the world's busiest areas for shipping activities (Chen et al., 2017). From Fig. 4, finer temporal patterns can be observed,

375 such as the gradual increase in emissions during the second half of 2017 and the subsequent decrease in ship emissions in 2019 as trade conflicts intensified. In 2020, the impact of the pandemic led to two phases of decline and recovery in global ship emissions. It is worth noting that CH_4 emissions exhibit relatively large daily changes and have been increasing throughout the six years. The primary source of

CH$_4$ emissions is LNG ships. The daily fluctuations in ship CH$_4$ emissions are mainly due to variations

380   in LNG ship activities. Although LNG ships are currently relatively few, their quantity is increasing as

the demand for low-carbon ships grows steadily (Gronholm et al., 2021).

3.2.2   Multi-dimensional structure
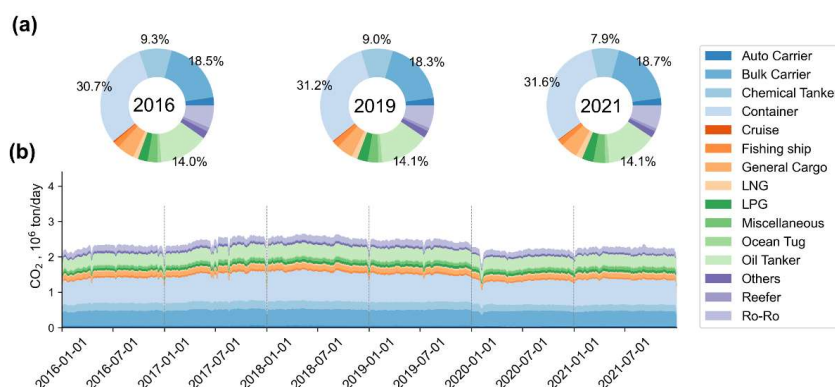
Figure 5: Composition of global ship CO$_2$ emissions by vessel type from 2016 to 2021. a) the percentage

385   contribution of emissions by vessel type for the years 2016, 2019, and 2021; b) the five-day moving average of

daily emissions for different vessel types.

Figure 5 displays the daily CO$_2$ emissions classified by vessel type. From 2016 to 2021, container

ships, bulk carriers, and oil tankers consistently contributed the most, accounting for 31.6%, 18.7%, and

14.1% of global ship CO$_2$ emissions in 2021, respectively. The contribution of container ships increased

390   from 30.7% to 31.6% from 2016 to 2021. Overall, there were no significant changes in the composition

of vessel types over the six years. Vessel types reflect the types of commodities transported by sea,

indicating the relative stability of the global maritime cargo structure.
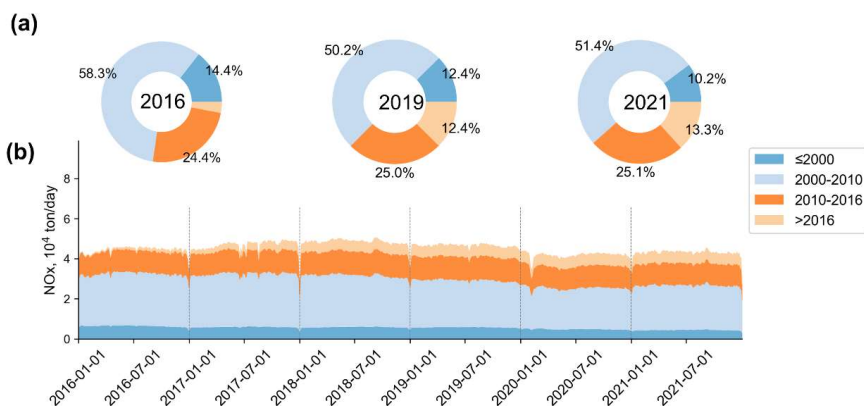
Figure 6: Composition of global ship NOₓ emissions by vessel construction year from 2016 to 2021. a) the
percentage contribution of emissions by vessels constructed in different periods for the years 2016, 2019, and 2021;
b) the five-day moving average of daily emissions for vessels constructed in different periods.

Figure 6 illustrates the daily NO_x emissions composed by the vessel construction period. The
construction year of vessels determines the NO_x emission standards followed by their engine(Imo, 2008).
From 2016 to 2021, vessels complying with Tier I standards (built during the year 2000-2010)
consistently contributed over 50% of ship NO_x emissions, while those complying with Tier II standards
(built during the year 2010-2015) contributed approximately half of Tier I emissions. As the majority of
ship NO_x emissions come from Tier I- and Tier II-standard vessels, global ship NO_x emissions are
expected to remain at current levels in the short term without further control measures. However, it is
noteworthy that the contribution of vessels over 20 years old (built-year $\leqslant$ 2000) to global ship NO_x
emissions has gradually decreased, from 14.4% in 2016 to 10.2% in 2021. Meanwhile, the contribution
of newly built vessels (built-year $\geqslant$ 2016) to global ship NO_x emissions has steadily increased from
3.5% in 2019 to 13.3% in 2021.

3.3 Spatial characteristics

3.3.1 High-resolution patterns

Based on latitude and longitude coordinates in AIS signals, the ship emissions dataset was spatially
aggregated into grids, resulting in the global spatial distribution of ship emissions. Figure 7 depicts the
SO_2 emissions from global ships in $0.1° \times 0.1°$ grids. The regions with high intensity of ship SO_2
emissions include East Asia, South Asia, Europe, the Persian Gulf, the Mediterranean, and the western
coast of Europe. The intensive ship emissions along major global shipping routes are clearly visible, such

415   as the routes connecting East Asia through the Malacca Strait, the Suez Canal, and the Strait of Hormuz

to Western European countries (the "Europe-Middle East-Far East route"), the Strait of Gibraltar, the

Strait of Hormuz, and the critical passage connecting the Pacific and Atlantic Oceans, the Panama Canal,

among others. Comparing the spatial distribution of ship SO_2 emissions in different years, noticeable

reductions in emissions are observed in ECAs such as North America, the Gulf of Mexico, the North Sea,

420   and the Baltic Sea comparing the ship SO_2 emissions distribution in 2013 and 2016. A significant

reduction in emissions is also observed in the Domestic Emission Control Area (DECA) comparing the

ship SO_2 emissions distribution in 2016 and 2019. In 2021, the implementation of the global low-sulfur

fuel policy resulted in a significant overall reduction in ship SO_2 emissions spatially compared with 2019.

The spatial distribution of ship SO_2 emissions in different years demonstrates that the SEIM v2.2

425   effectively responds to SO_2 emission control policies.
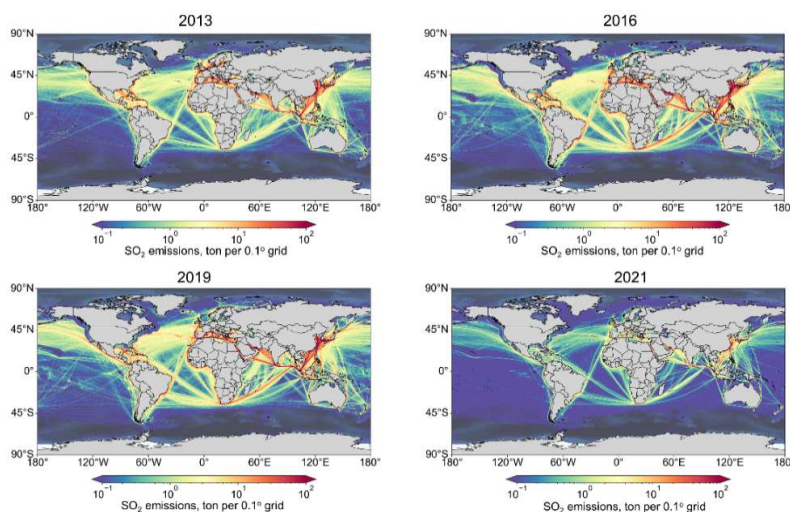
Figure 7: Spatial distribution of global ship SO₂ emissions in different years

3.3.2   Spatial disparities of vessel composition

Distinct disparities in spatial distribution are evident between freight vessels and non-freight

430   vessels in Fig. 8. Emissions from container ships, bulk carriers, and oil tankers are concentrated in major

international shipping lanes. In contrast, emissions from non-transport vessels such as fishing vessels are

more widely distributed in non-lane open sea areas. According to this study, in 2021, fishing vessels

contributed 1.6% to global ship CO_2 emissions, with their emissions mainly concentrated in the North
Sea, Baltic Sea, Yellow Sea, and South Pacific. In recent years, studies have utilized fine satellite data to
435   reveal significant fishing vessel activities that had not been publicly tracked worldwide (Paolo et al.,
2024). The emissions from those fishing vessels remain unknown. Therefore, the emissions from fishing
vessels presented in this study should be considered highly uncertain and are not discussed in the
following sections.
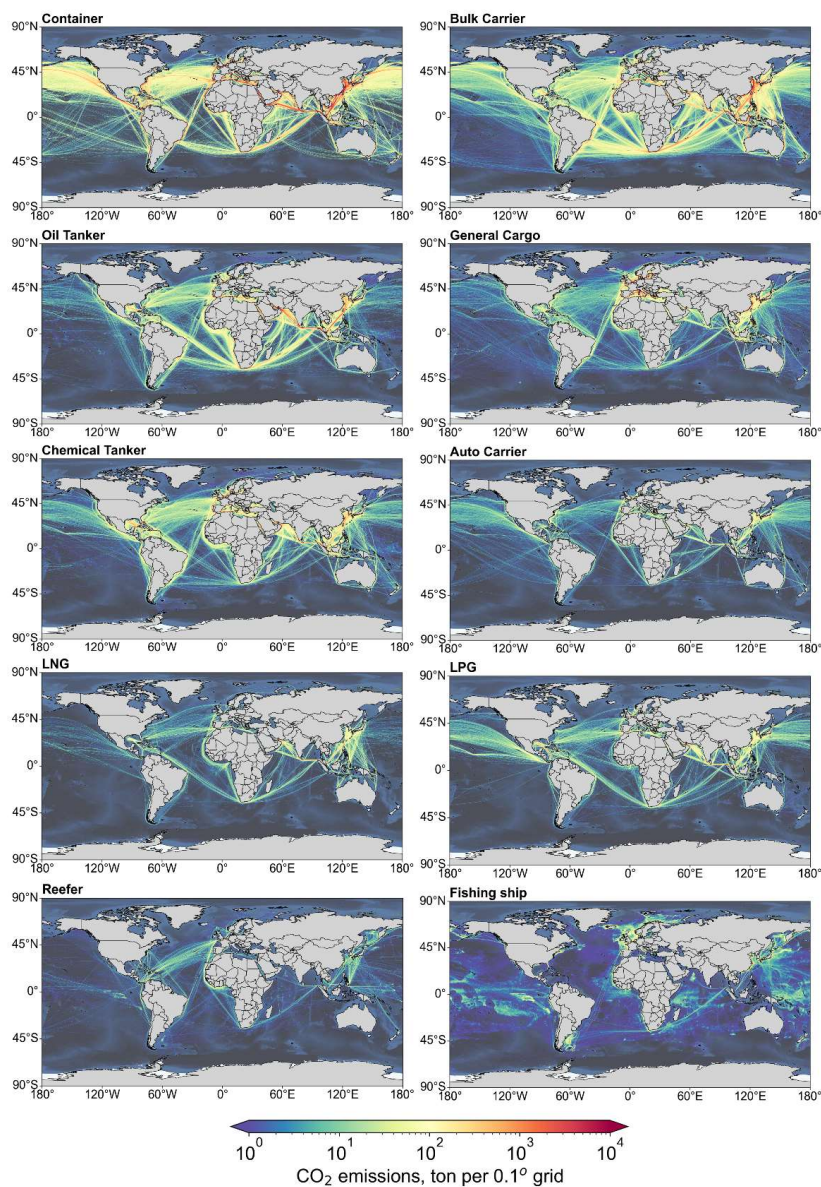
Figure 8: Spatial distribution of CO$_2$ emissions from different types of vessels in 2021

The spatial distribution of emissions varies across different vessel types, leading to disparities in the composition of vessel types in different maritime regions. The division of global maritime regions is based on the International Hydrographic Organization (IHO) standards (https://iho.int/). Figure 9

illustrates the composition of vessel types in the top 14 regions with the highest CO_2 emissions globally

445   in 2021, with their combined emissions accounting for almost 80% of the total global emissions. In the

pie charts for each region, vessel types contributing over 10% of emissions are labeled. It is observed

that container ships contribute significant emissions in the North Pacific Ocean, South China Sea, and

East China Sea, accounting for 49.4%, 37.4%, and 38.7% respectively, well above the global average

(31.6%). Regions with high contributions from bulk carriers are mainly distributed in the southern

450   hemisphere, such as the Indian Ocean (40.7%) and South Atlantic (34.9%). Ro-Ro vessels exhibit high

emissions proportions near Europe, with percentages of 38.7% in the Baltic Sea, 19.3% in the North Sea,

and 18.1% in the Mediterranean. Oil tankers contribute 28.5% of emissions in the Arabian Sea, probably

attributed to countries like Saudi Arabia and Iran, rich in oil and gas resources, generating substantial

shipping emissions during exports to other countries.
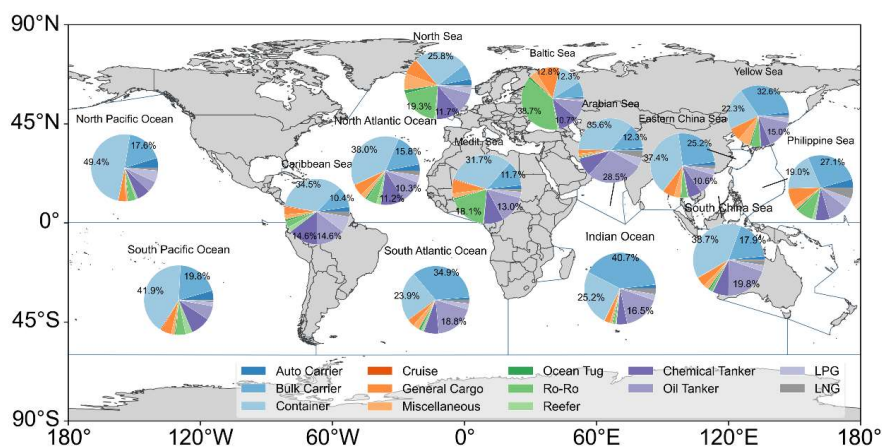
455

Figure 9: Ship CO₂ emissions composition in different maritime regions globally in 2021 (excluding fishing ships and others)

3.3.3 Emission intensity
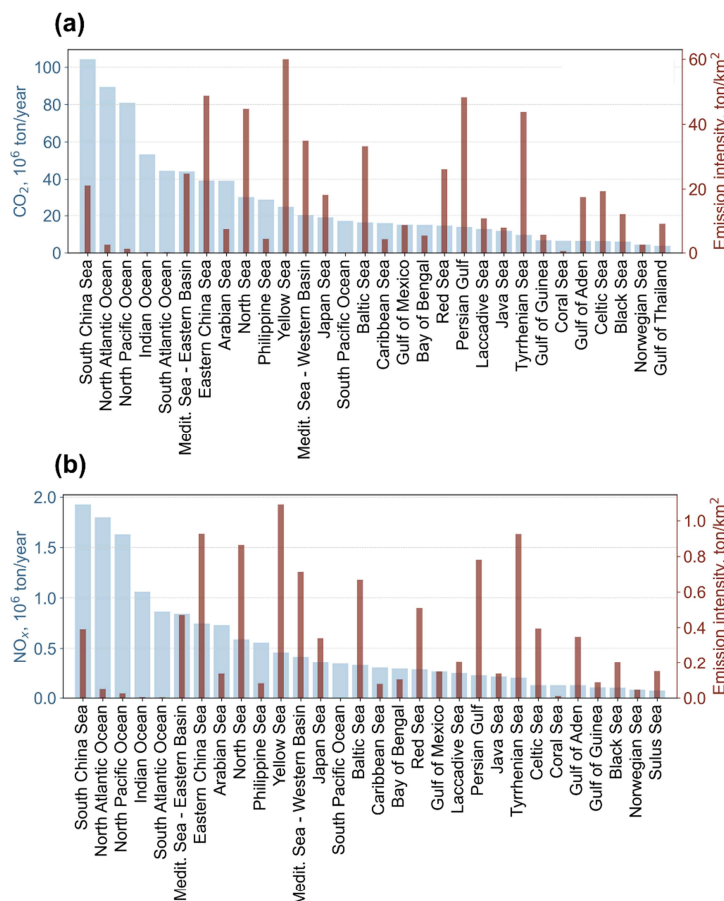
Figure 10: Global ship (a) CO$_2$ and (b) NO$_x$ emission and emission intensities in different maritime regions in 2021

Since the significant differences in the area of 0.1°×0.1° grids at different latitudes, ship emissions within each grid are standardized into emission intensity, i.e., emissions per unit area (unit: ton/km^2). Taking ship CO$_2$ emissions as an example, Fig. 10 illustrates the total ship CO$_2$ emissions and emission intensity in major maritime regions in 2021. The top 30 maritime regions with the highest CO$_2$ and NO$_x$ emissions, accounting for approximately 96% of the total global ship emissions, are listed and arranged in descending order of total emissions. It is important to note that the South/North Pacific, South/North Atlantic, and Indian Ocean cover a vast area (about 75% of the total maritime area), most of which have

little or no ship navigation. Calculating the total average emission intensity for these regions would

470 weaken their significance, so they are not discussed here. Among other maritime regions, the South China

Sea has the highest total ship CO_2 and NO_x emissions. As a vital route for maritime trade between East

Asia Europe and Africa, the South China Sea exhibits prominent ship traffic density globally.

Additionally, the Eastern Mediterranean Basin, the Arabian Sea, the East China Sea, the Philippine Sea,

and the North Sea also have relatively significant total emissions. Generally, maritime regions with high

475 CO_2 emissions also have relatively high NO_x emissions. Although the order of maritime regions with

lower emissions differs slightly, overall consistency is observed. There are significant differences

between maritime regions with high emissions and those with high emission intensity. The top five

maritime regions with the highest ship CO_2 emission intensity are the Yellow Sea, the Persian Gulf, the

East China Sea, the North Sea, and the Tyrrhenian Sea. The top five for NO_x emission intensity are also

480 the same maritime regions. These regions are coastal areas or busy maritime routes with intensive ship

emissions, which warrants attention in environmental management in the future.

4   Data Availability

Shipping emission data described in this manuscript can be accessed at Zenodo under
https://zenodo.org/records/11069531 (Wen et al., 2024).

485 ## 5   Conclusions

Utilizing the SEIM model, we developed a high-resolution ship emission inventory covering the

period from 2013 to 2016-2021 globally, encompassing 5 atmospheric pollutants (NO_x, SO_2, $PM_{2.5}$, CO,

HC) and 4 greenhouse gases (CO_2, CH_4, N_2O, BC). With a temporal resolution of day and spatial

resolution of 0.1º $\times$ 0.1º, our inventory revealed novel insights into global ship emission characteristics.

490 In terms of annual emissions, our inventory exhibits consistency in temporal trends and emission

magnitudes compared to mainstream inventory datasets including EDGAR, CEDS, and IMO. According

to this study and the global anthropogenic emission inventory by (Hoesly Rachel, 2024), ship emissions

contributed 12.3% of SO_2, 14.0% of NO_x, and 2.5% of CO_2 to global anthropogenic emissions in 2019,

and 3.2% of SO_2, 14.2% of NO_x, and 2.3% of CO_2 to global anthropogenic emissions in 2021. Over the years, ship CO_2, NO_x, CO, HC, and N_2O emissions showed a declining trend due to the impacts of the 2019 trade conflict (year-on-year decrease rate 5.4%-6.2%) and the 2020 pandemic (year-on-year decrease rate 7.4%-13.8%), with a subsequent rebound in 2021 as international trade increased (year-on-year increase rate 3.1%-3.6%). SOx, PM, and BC emissions were significantly influenced by gradually implemented ECA policies and the 2020 low-sulfur fuel-switching policy. SOx and PM emissions in 2021 were 80.9% and 76.0% of those in 2019, and BC emissions were 38.7% of those in 2019. CH_4 emissions exhibited an increasing trend over the years, growing by 43.5% in 2021 compared to 2016.

Regarding emission composition, container ships consistently constituted the primary source of global ship CO_2 emissions, contributing over 30% annually and steadily increasing, followed by bulk carriers, oil tankers, and chemical tankers. The proportion of emissions contributed by new ships increased annually from 3.5% in 2016 to 13.3% in 2021. However, Tier I and Tier II ships still dominate ship NO_x emissions. Currently, Tier III standards only apply to vessels operating in North American Emission Control Areas. Achieving a significant reduction in global ship NO_x emissions still requires extensive advancements in ship engine technology and follow-up regulatory measures worldwide.

As for spatial characteristics, ship emissions were particularly significant in East Asia, South Asia, and Europe, with busy shipping routes such as the Western Europe-Middle East-Far East route, the Strait of Malacca, the Strait of Gibraltar, the Strait of Hormuz, and the Panama Canal showing the highest emission intensities. Furthermore, influenced by the types of commodities transported and the countries involved in trade, significant differences in ship emission characteristics exist across different regions. SEIM enables the analysis of the heterogeneity of spatial distributions of ship emissions. In terms of vessel type composition, container ships significantly exceeded the global average in ship CO_2 emissions contributions in the North Pacific, East China Sea, and South China Sea. Regions with high proportions of emissions from bulk carriers were mainly located in the Southern Hemisphere, such as the Indian Ocean, South Pacific, and South Atlantic. Emissions from oil tankers were high in the Arabian Sea and the Persian Gulf. The regions with the highest CO_2 and NO_x ship emission intensities were the Yellow Sea, the Persian Gulf, the East China Sea, the North Sea, and the Tyrrhenian Sea.

Overall, SEIM offers a globally multi-year, high spatiotemporal resolution ship emission inventory that provides reliable and detailed data, which could support foundational research across disciplines such as atmospheric science, environmental science, and geoscience. Meanwhile, this dataset could also provide scientific support for facilitating shipping emission mitigation in the future.

525 **Acknowledgments**

This work was supported by the National Natural Science Foundation of China (grant nos. 42325505), National Key Research and Development Program of China (No. 2023YFC3705604 and No. 2022YFC3704200), and China Postdoctoral Science Foundation (No. 42305125).

Author contributions

530 W.Y. and X.W designed the research and wrote the manuscript, H.L. reviewed and revised the manuscript, and T.H. contributed to the modelling. Z.L. and Z.L. contributed to data analysis. K.H. and H.L. provided insights into the research design. All authors contributed to the writing.

Competing interests

The authors declare no competing interests.

535 **References**

Browse, J., Carslaw, K. S., Schmidt, A., and Corbett, J. J.: Impact of future Arctic shipping on high-latitude black carbon deposition, Geophysical Research Letters, 40, 4459-4463, https://doi.org/10.1002/grl.50876, 2013.
Chen, D., Wang, X., Li, Y., Lang, J., Zhou, Y., Guo, X., and Zhao, Y.: High-spatiotemporal-resolution
540 ship emission inventory of China based on AIS data in 2014, Science of The Total Environment, 609, 776-787, 10.1016/j.scitotenv.2017.07.051, 2017.
Chen, D., Fu, X., Guo, X., Lang, J., Zhou, Y., Li, Y., Liu, B., and Wang, W.: The impact of ship emissions on nitrogen and sulfur deposition in China, Science of The Total Environment, 708, 134636, https://doi.org/10.1016/j.scitotenv.2019.134636, 2020.
545 Chen, X. and Yang, J.: Analysis of the uncertainty of the AIS-based bottom-up approach for estimating ship emissions, Marine Pollution Bulletin, 199, 115968, https://doi.org/10.1016/j.marpolbul.2023.115968, 2024.

Corbett, J. J., Fischbeck, P. S., and Pandis, S. N.: Global nitrogen and sulfur inventories for oceangoing ships, Journal of Geophysical Research: Atmospheres, 104, 3457-3470, 10.1029/1998jd100040, 1999.

550   Crippa, M., Guizzardi, D., Solazzo, E., Muntean, M., Schaaf, E., Monforti-Ferrario: GHG emissions of all world countries - 2021 Report, Luxembourg, 2021.

Development, t. U. N. C. o. T. a.: Review of Maritime Transport,   2023.

Diamond, M. S.: Detection of large-scale cloud microphysical changes within a major shipping corridor after implementation of the International Maritime Organization 2020 fuel sulfur regulations, Atmos.

555   Chem. Phys., 23, 8259-8269, 10.5194/acp-23-8259-2023, 2023.

DNV: Maritime Forcast to 2050, 2022.

Emmens, T., Amrit, C., Abdi, A., and Ghosh, M.: The promises and perils of Automatic Identification System   data,   Expert   Systems   with   Applications,   178,   114975, https://doi.org/10.1016/j.eswa.2021.114975, 2021.

560   Endresen, O., Sorgard, E., Sundet, J. K., Dalsoren, S. B., Isaksen, I. S. A., Berglen, T. F., and Gravir, G.: Emission from international sea transportation and environmental impact, Journal of Geophysical Research-Atmospheres, 108, 10.1029/2002jd002898, 2003.

Eyring, V., Isaksen, I. S. A., Berntsen, T., Collins, W. J., Corbett, J. J., Endresen, O., Grainger, R. G., Moldanova, J., Schlager, H., and Stevenson, D. S.: Transport impacts on atmosphere and climate:

565   Shipping, Atmospheric Environment, 44, 4735-4771, 10.1016/j.atmosenv.2009.04.059, 2010.

Fu, M., Liu, H., Jin, X., and He, K.: National- to port-level inventories of shipping emissions in China, Environmental Research Letters, 12, 10.1088/1748-9326/aa897a, 2017.

Fu, X., Chen, D., Guo, X., Lang, J., and Zhou, Y.: Improving the estimation of ship emissions using the high-spatiotemporal resolution wind fields simulated by the Weather Research and Forecast model: A

570   case study in China, Journal of Industrial Ecology, 26, 1871-1881, https://doi.org/10.1111/jiec.13278, 2022.

Gronholm, T., Makela, T., Hatakka, J., Jalkanen, J. P., Kuula, J., Laurila, T., Laakso, L., and Kukkonen, J.: Evaluation of Methane Emissions Originating from LNG Ships Based on the Measurements at a Remote Marine Station, Environ Sci Technol, 55, 13677-13686, 10.1021/acs.est.1c03293, 2021.

575   Hoesly Rachel, S. S.: CEDS v_2024_04_01 Release Emission Data (v_2024_04_01) Zenodo [dataset], https://doi.org/10.5281/zenodo.10904361, 2024.

IMO: Amendents to the techincal code on control of emission of nitrogen oxides from marine diesel engines, 2008.

IMO: Further technical and operational measures for enhancing the energy efficiency of international

580   shipping, 2015.

Jalkanen, J. P., Johansson, L., Kukkonen, J., Brink, A., Kalli, J., and Stipa, T.: Extension of an assessment model of ship traffic exhaust emissions for particulate matter and carbon monoxide, Atmospheric Chemistry and Physics, 12, 2641-2659, 10.5194/acp-12-2641-2012, 2012.

Jasper Faber, S. H., Shuang Zhang, Paula Pereda, Bryan Comer: Forth IMO Greenhouse gas study,

585   London, 2020.

Johansson, L., Jalkanen, J.-P., and Kukkonen, J.: Global assessment of shipping emissions in 2015 on a high   spatial   and   temporal   resolution,   Atmospheric   Environment,   167,   403-415, 10.1016/j.atmosenv.2017.08.042, 2017.

Kersey, J., Popovich, N. D., and Phadke, A. A.: Rapid battery cost declines accelerate the prospects of
590   all-electric interregional container shipping, Nature Energy, 7, 664-674, 10.1038/s41560-022-01065-y,
2022.

Kramel, D., Muri, H., Kim, Y., Lonka, R., Nielsen, J. B., Ringvold, A. L., Bouman, E. A., Steen, S., and
Strømman, A. H.: Global Shipping Emissions from a Well-to-Wake Perspective: The MariTEAM Model,
Environmental Science & Technology, 55, 15040-15050, 10.1021/acs.est.1c03937, 2021.

595   Liu, H., Fu, M., Jin, X., Shang, Y., Shindell, D., Faluvegi, G., Shindell, C., and He, K.: Health and climate
impacts of ocean-going vessels in East Asia, Nature Climate Change, 6, 1037-1041,
10.1038/nclimate3083, 2016.

Liu, H., Yi, W., Jalkanen, J.-P., Luo, Z., Majamäki, E., Matthias, V., Moldanová, J., Shi, Z., and He, K.:
Atmospheric impacts and regulation framework of shipping emissions: achievements, challenges and
600   frontiers, Fundamental Research, https://doi.org/10.1016/j.fmre.2024.02.013, 2024.

Luo, Z., He, T., Yi, W., Zhao, J., Zhang, Z., Wang, Y., Liu, H., and He, K.: Advancing shipping NOx
pollution   estimation   through   a   satellite-based   approach,   PNAS   Nexus,   pgad430,
10.1093/pnasnexus/pgad430, 2023.

Luo, Z., Lv, Z., Zhao, J., Sun, H., He, T., Yi, W., Zhang, Z., He, K., and Liu, H.: Shipping-related
605   pollution decreased but mortality increased in Chinese port cities, Nature Cities, 1, 295-304,
10.1038/s44284-024-00050-8, 2024.

McDuffie, E. E., Smith, S. J., O'Rourke, P., Tibrewal, K., Venkataraman, C., Marais, E. A., Zheng, B.,
Crippa, M., Brauer, M., and Martin, R. V.: A global anthropogenic emission inventory of atmospheric
pollutants from sector- and fuel-specific sources (1970–2017): an application of the Community
610   Emissions Data System (CEDS), Earth System Science Data, 12, 3413-3442, 10.5194/essd-12-3413-
2020, 2020.

Paolo, F. S., Kroodsma, D., Raynor, J., Hochberg, T., Davis, P., Cleary, J., Marsaglia, L., Orofino, S.,
Thomas, C., and Halpin, P.: Satellite mapping reveals extensive industrial activity at sea, Nature, 625,
85-91, 10.1038/s41586-023-06825-8, 2024.

615   Smith, T. W. P. J., J. P.; Anderson, B. A.; Corbett, J. J.; Faber, J.; Hanayama: Third IMO GHG Study,
London, 2014.

Sou, W. S., Goh, T., Lee, X. N., Ng, S. H., and Chai, K.-H.: Reducing the carbon intensity of international
shipping – The impact of energy efficiency measures, Energy Policy, 170, 10.1016/j.enpol.2022.113239,
2022.

620   Stephenson, S. R., Wang, W., Zender, C. S., Wang, H., Davis, S. J., and Rasch, P. J.: Climatic Responses
to Future Trans-Arctic Shipping, Geophys Res Lett, 45, 9898-9908, 10.1029/2018GL078969, 2018.

Wang, X., Yi, W., Lv, Z., Deng, F., Zheng, S., Xu, H., Zhao, J., Liu, H., and He, K.: Ship emissions
around China under gradually promoted control policies from 2016 to 2019, Atmospheric Chemistry and
Physics, 21, 13835-13853, 10.5194/acp-21-13835-2021, 2021.

625   Wen, Y., Xiaotong, W., Tingkun, H., Huan, L., Luo, Z., and Kebin, H.: Global shipping emissions for
the years 2013 and 2016-2021, Zenodo [dataset], 10.5281/zenodo.10869014, 2024.

Yuan, T., Song, H., Wood, R., Wang, C., Oreopoulos, L., Platnick, S. E., von Hippel, S., Meyer, K.,
Light, S., and Wilcox, E.: Global reduction in ship-tracks from sulfur regulations for shipping fuel,
Science Advances, 8, eabn7988, 10.1126/sciadv.abn7988, 2022.

630   Zhang, C., Shi, Z., Zhao, J., Zhang, Y., Yu, Y., Mu, Y., Yao, X., Feng, L., Zhang, F., Chen, Y., Liu, X.,
       Shi, J., and Gao, H.: Impact of air emissions from shipping on marine phytoplankton growth, Science of
       The Total Environment, 769, 145488, https://doi.org/10.1016/j.scitotenv.2021.145488, 2021.
       Zhang, Q., Wan, Z., Hemmings, B., and Abbasov, F.: Reducing black carbon emissions from Arctic
       shipping: Solutions and policy implications, Journal of Cleaner Production, 241,
635   10.1016/j.jclepro.2019.118261, 2019.